Applied Physics Letters

RESEARCH ARTICLE | JUNE 01 2026

Antisymmetric planar Hall effect in Ta/Py bilayers—Evidence for perpendicular interfacial magnetization tuned by in-plane bulk magnetization

A. Ghosh ; A. Zaig ; D. B. C. Gonçalves ; S. Cardoso ; L. Klein

Check for updates

Appl. Phys. Lett. 128, 221601 (2026)
https://doi.org/10.1063/5.0326432

View Online
Export Citation

27 October 2026 10:58:36

Nanotechnology & Materials Science
Optics & Photonics
Impedance Analysis
Scanning Probe Microscopy
Sensors
Failure Analysis & Semiconductors

Unlock the Full Spectrum.
From DC to 8.5 GHz.



Zurich Instruments

Find out more

AIP Publishing

Applied Physics Letters ARTICLE pubs.aip.org/aip/apl

Antisymmetric planar Hall effect in Ta/Py bilayers—Evidence for perpendicular interfacial magnetization tuned by in-plane bulk magnetization

Cite as: Appl. Phys. Lett. **128**, 221601 (2026); doi: 10.1063/5.0326432
Submitted: 5 February 2026 · Accepted: 14 May 2026 ·
Published Online: 1 June 2026

View Online Export Citation CrossMark

A. Ghosh,[1,a] A. Zaig,[1] D. B. C. Gonçalves,[2,3] S. Cardoso,[2,3] and L. Klein[1,b]

AFFILIATIONS

[1]Department of Physics, Institute of Nanotechnology and Advanced Materials, Bar-Ilan University, Ramat-Gan 5290002, Israel
[2]Instituto de Engenharia de Sistemas e Computadores—Microsistemas e Nanotecnologias (INESC MN), Lisbon, Portugal
[3]Instituto Superior Técnico, Universidade de Lisboa, 1649-004 Lisboa, Portugal

[a]Author to whom correspondence should be addressed: arupghoshphy@gmail.com
[b]Electronic mail: lior.klein@biu.ac.il

ABSTRACT

Antisymmetric planar Hall effect (APHE) is observed in Ta/Py bilayers, which exhibits a sinusoidal dependence on the in-plane magnetization orientation. The APHE resistance is independent of both the amplitude and direction of the applied current, excluding contributions from Joule heating and spin–orbit torque effects. Additionally, the effect is insensitive to the magnitude of the in-plane magnetic field once the magnetization is practically saturated. The APHE amplitude and phase vary with the choice of seed layer and with post-deposition annealing, suggesting involvement of strain. Results suggest the presence of strain-modulated interfacial Dzyaloshinskii–Moriya interaction, which couples the bulk and interfacial spins and induces perpendicular magnetization at the Ta/Py interface tuned by the orientation of the in-plane bulk magnetization: a miter-gear-like combination. This mechanism offers a plausible explanation for the antisymmetric Hall response and points to a new pathway for inducing and manipulating perpendicular interfacial magnetization, with potential implications for novel spintronic devices.

© 2026 Author(s). All article content, except where otherwise noted, is licensed under a Creative Commons Attribution (CC BY) license (https://creativecommons.org/licenses/by/4.0/). https://doi.org/10.1063/5.0326432

27 October 2026 10:58:36

Heterostructures combining heavy metal (HM) and ferromagnetic (FM) layers exhibit intriguing phenomena, including perpendicular magnetic anisotropy (PMA),[1–4] spin–orbit torque (SOT),[5–8] spin Hall effect (SHE),[9,10] and proximity-induced magnetization.[11] Additionally, spin–orbit coupling (SOC) combined with broken inversion symmetry at such interfaces gives rise to the Dzyaloshinskii–Moriya interaction (DMI),[12–15] which favors canted spin configurations with a defined chirality. DMI has attracted great interest, particularly due to its connection to the stabilization of topologically nontrivial spin textures such as skyrmions, which are explored as potential building blocks for next-generation spintronic memory and logic devices.[16–18] The strength and character of interfacial DMI depend sensitively on structural factors, including layer thickness, interface roughness, and the choice of seeding or buffer layers, all of which modify the local crystal symmetry and magnetic anisotropy.[18–25]

While DMI has been extensively investigated in thin films and multilayers exhibiting PMA,[12–25] its presence and effects are far less explored in systems exhibiting in-plane magnetic anisotropy (IMA).[26–28] In PMA systems, interfacial DMI is readily manifested through the formation of chiral spin textures and domain-wall dynamics, providing clear experimental signatures.[16–18] In contrast, DMI is more subtle and often difficult to detect directly in IMA systems, as the in-plane alignment of magnetization tends to suppress out-of-plane spin canting.[29,30] Nevertheless, theoretical and experimental studies have suggested that, also in such systems, interfacial symmetry breaking and/or strain are expected to induce interfacial perpendicular magnetization.[26,30]

Recently, the antisymmetric planar Hall effect (APHE) has been used to detect perpendicular magnetization components.[31–39] APHE can arise from distinct microscopic routes and, critically, provide a sensitive electrical probe of tiny out-of-plane spin canting. In topological semimetals (e.g., WTe_2), planar Hall-type signals have been tied to Berry-curvature/chiral-anomaly physics.[35] In oxide heterostructures and rutile oxides (RuO_2, IrO_2), APHE has been observed due to

© Author(s) 2026

a symmetry-constrained Lorentz force mechanism.[34,39] At SOC rich interfaces, theory shows that SOC-induced canting (and related anisotropies) can generate anisotropic/antisymmetric planar Hall voltages, positioning APHE as a practical readout of interfacial spin tilts that are difficult to access by bulk magnetometry.[40]

Here, we observe APHE resistance in Ta(5 nm)/Py(2 nm) bilayers that exhibit IMA.[41,42] The signal is consistent with a small perpendicular magnetization localized at the Ta/Py interface. By engineering interfacial symmetry via seed layers (SiO_2, MgO, and Al_2O_3) and post-growth annealing, we tune the amplitude and phase of the APHE. The signal is insensitive to field magnitude yet tightly linked to the orientation of the in-plane bulk magnetization and free from spin–orbit torque and Joule-heating artifacts. The results point to a strain-modulated interfacial DMI that couples bulk and interfacial spins, particularly in the low-strain film grown on Al_2O_3 (40 nm) seed layers. Further strain relaxation upon annealing enhances the antisymmetric response in the same film. These results establish Ta/Py as a promising IMA platform in which interfacial DMI offers a practical route to unveil a previously unexplored pathway for inducing and manipulating perpendicular interfacial magnetization in HM/FM bilayers, offering new opportunities for the design and development of advanced multistate spintronic devices.

Multilayer stacks of Ta(5 nm)/Py(2 nm)/Ti(3 nm) and Ta(5 nm)/Py(2 nm)/MgO(3 nm)/Ta(2 nm) were deposited on Si/SiO_2(100 nm) substrates using ion beam deposition (IBD, Nordiko 3600) and magnetron sputtering techniques (Nordiko 8800). Both deposition modules are incorporated into a multi-chamber system, allowing for transfer without a vacuum break. Seed layers of MgO and Al_2O_3 were deposited by magnetron sputtering. Hall bars ($1 \times 0.1\ mm^2$) were fabricated from the above-mentioned multilayers by two-step laser photolithography. In step 1, the Hall-bar geometry was patterned and etched using Ar-ion milling to define the magnetic structures. In step 2, Cr(5 nm)/Au(50 nm) contact pads were patterned and subsequently deposited by magnetron sputtering, followed by lift-off. Grazing-incidence x-ray diffraction (GI-XRD, Cu-K_α, $\lambda = 1.540\,56$ Å) 2θ scans were recorded in a Rigaku Smartlab x-ray diffractometer (results are given in supplementary material Sec. S1.6). Planar Hall effect (PHE) measurements were performed in a laboratory-built setup incorporating two mutually orthogonal pairs of Helmholtz coils, each driven by an independent bipolar power supply, to generate in-plane magnetic-field components H_x and H_y. Field-magnitude (H) and angle (ϕ) were swept by varying the coil currents, where we define $H = \sqrt{H_x^2 + H_y^2}$ and $\phi = \text{atan2}(H_y, H_x)$.

Figure 1 presents planar Hall effect (PHE) measurements on Hall bars fabricated from an Al_2O_3(35 nm)/Ta(5 nm)/Py(2 nm)/Ti(3 nm) stack. In Fig. 1(a), the PHE resistance (R_{PHE}) is plotted as a function of the angle ($\phi_{current}$) of a 40 Oe in-plane magnetic field (H) relative to the direction of current (I). For this field, the in-plane magnetization (M_{in}) is parallel to H. Normally, PHE follows $R_{PHE} = R_0 \sin(2\phi)$; where R_0 is a constant and ϕ is the angle between the applied I and M_{in}; namely, it is symmetric under magnetization reversal ($\vec{M}_{in} \rightarrow -\vec{M}_{in}$).[41,43] Nevertheless, we note that the peak values of R_{PHE} at 45°, 135°, 225°, and 315° are not identical, suggesting an antisymmetric contribution. To separate the symmetric (SPHE) and antisymmetric (APHE) contributions to the PHE signals, we use the reciprocity theorem $R_{PHE}^{12,34}(+H) = R_{PHE}^{34,12}(-H)$, where the first index pair (1–2 or 3–4) denotes the current leads and the second pair denotes the voltage leads.[44,45] By exchanging current and voltage leads, we obtain $R_{PHE}^{S} = (R_{PHE}^{12,34} + R_{PHE}^{34,12})/2$ and $R_{PHE}^{AS} = (R_{PHE}^{12,34} - R_{PHE}^{34,12})/2$, shown in Figs. 1(b) and 1(c). More details on the decomposition of SPHE and APHE are given in supplementary material Sec. S1.1 (Fig. S1). The symmetric component follows $R_{PHE}^{S} = R_0^{S} \sin(2\phi)$, whereas the antisymmetric component can be described by $R_{PHE}^{AS} = R_0^{AS} \cos(\phi - \phi_0^{AS})$, where R_0^{S} and R_0^{AS} are the amplitudes of SPHE and APHE and ϕ_0^{AS} is the angle where R_{PHE}^{AS} attains its maximum. The inset of Fig. 1(c) displays $R_{PHE}^{AS}(H)$ for field sweeps taken at angles near the minimum ($\phi_{current} \sim 145°$) and maximum ($\phi_{current} \sim 55°$) of the APHE response. R_{PHE}^{AS} remains close to zero at 145° but increases and saturates at 55°. To explore the origin of the antisymmetric component, we study its dependence on various parameters.

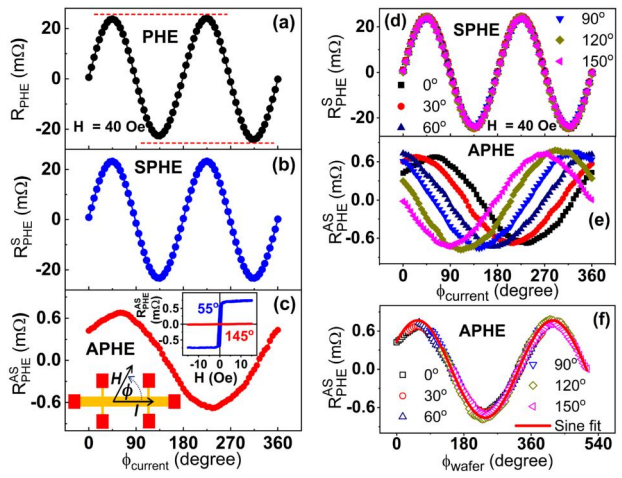


FIG. 1. (a) PHE resistance (R_{PHE}) for a Hall bar fabricated from an Al_2O_3(35 nm)/Ta(5 nm)/Py(2 nm)/Ti(3 nm) stack, plotted vs the in-plane field angle defined relative to the current ($\phi_{current}$). (b) Symmetric (R_{PHE}^{S}) and (c) antisymmetric (R_{PHE}^{AS}) components of R_{PHE}. Lower inset: Schematic of a Hall bar and measurement configuration. Upper inset: Field dependence of R_{PHE}^{AS} for in-plane sweeps at 55° and 145°. In-plane angle sweeps of (d) R_{PHE}^{S} and (e) R_{PHE}^{AS} measured in Hall bars oriented at $\alpha_{wafer} = 0°$–150° in 30° steps relative to the wafer edge. (f) R_{PHE}^{AS} replotted as a function of the wafer-fixed angle ϕ_{wafer}, defined with respect to the current direction of the Hall bar at $\alpha_{wafer} = 0°$.

To find out whether R_{PHE}^{AS} depends on $\phi_{current}$ (as R_{PHE}^{S}), we fabricated Hall bars patterned at different angles relative to the wafer's edge, $\alpha_{wafer} = 0°$, 30°, 60°, 90°, 120°, and 150°. Figures 1(d) and 1(e) show R_{PHE}^{S} and R_{PHE}^{AS}, respectively, for the above-mentioned orientations. As expected, R_{PHE}^{S} of all the Hall bars collapse onto a single curve when plotted against the angle between M_{in} and I ($\sim \phi_{current}$). In contrast, R_{PHE}^{AS} exhibits a monotonic shift in its peak position with α_{wafer}. However, the curves nearly coincide and exhibit a common maximum when the data in Fig. 1(e) are replotted in Fig. 1(f) vs ϕ_{wafer}, defined as the angle between M_{in} and a fixed reference direction in the wafer plane. Here, that reference direction was chosen arbitrarily as the current direction of the Hall bar with $\alpha_{wafer} = 0°$. This collapse shows that R_{PHE}^{AS} is governed by a wafer-fixed structural axis rather than by the current direction. To reinforce this result, we tested this behavior in a pattern with three-crossing ellipses,[41] where

27 October 2026 10:58:36

© Author(s) 2026

the I is driven to the same region in different directions. The outcome was unchanged—the relevant angle is between M_{in} and a wafer-fixed axis, independent of the direction of I (see Fig. S2 in the supplementary material).

The dependence of R^{AS}_{PHE} on current amplitude is shown in Fig. 2, which presents the in-plane angle dependence of R^{AS}_{PHE} measured at $H = 40$ Oe for different values of I applied to a Hall bar. Neither R^{AS}_{PHE} nor R^{S}_{PHE} (inset) shows any discernible dependence on the magnitude of I. The demonstrated insensitivity to current direction and amplitude excludes mechanisms rooted in spin–orbit torques or Joule-heating–driven thermoelectric effects (e.g., Nernst-type signals).[46–48] We also note that the amplitude of APHE is suppressed by $\sim 50\times$ in an otherwise similar wafer with a 10 nm Py layer [Fig. S3(b) in the supplementary material], consistent with an interface-dominated origin that is most pronounced for ultrathin Py.

Figures 3(a) and 3(b) show the angle dependence of R^{S}_{PHE} and R^{AS}_{PHE} measured under selected values of H applied in-plane. As H increases, the amplitude of R^{S}_{PHE} grows and approaches saturation, consistent with improved alignment of M_{in}. In contrast, R^{AS}_{PHE} remains essentially unchanged in amplitude over the same field range, indicating that the APHE is governed primarily by the orientation of M_{in} rather than the magnitude of H. This field insensitivity also excludes artifacts such as an unintended out-of-plane field component caused by a slight mechanical tilt of the sample stage or Helmholtz coils. Figure 3(c) shows R^{S}_{PHE} and R^{AS}_{PHE} in a Hall bar as a function of in-plane field measured at $\phi_{current} = 135°$. Sharp cusps in R^{S}_{PHE} at $H \approx \pm 1$ Oe mark the coercive field of the Py layer at which M_{in} switches its direction with field reversal and concomitantly R^{AS}_{PHE} flips sign as well. Together, these observations establish the link between the antisymmetric component and the in-plane magnetization direction.

Figure 3(d) presents the antisymmetric Hall resistance (R^{AS}_{Hall}) measured while sweeping the out-of-plane field magnitude H_z (see inset), with the in-plane magnetization locked at selected angles by a constant in-plane bias $H_{xy} = 40$ Oe. All the traces are linear in H_z with an identical slope. The curves are simply offset vertically by an amount equal to the APHE magnitude at the corresponding in-plane angle [i.e., the $H_z = 0$ intercept reproduces $R^{AS}_{PHE}(\phi_{current})$]. Namely, the Hall effect due to the perpendicular field and the APHE add up, and the APHE is not affected by the perpendicular field at least in the range of ± 40 Oe.

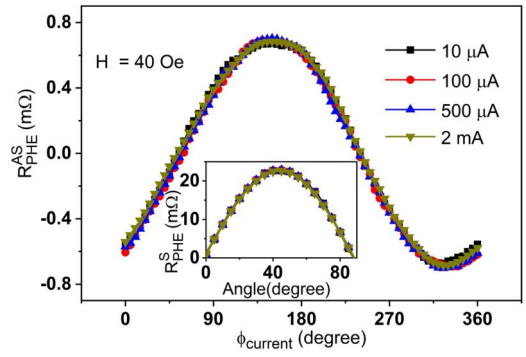


FIG. 2. R^{AS}_{PHE} as a function of in-plane angle of $H = 40$ Oe measured with different current values ($I = 10$, 100, 500 μA, and 2 mA) applied to the Hall bar. Inset: Corresponding R^{S}_{PHE} vs $\phi_{current}$ measured for the same current values.

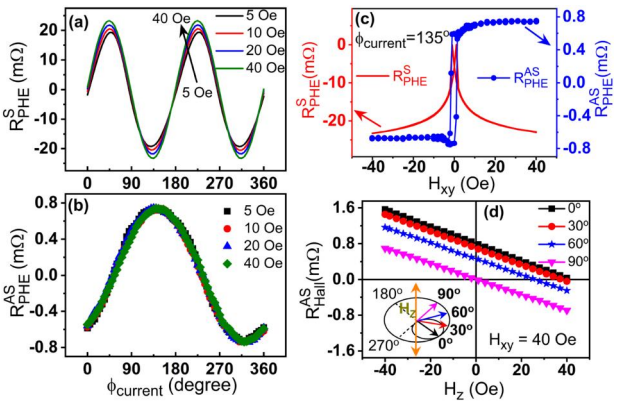


FIG. 3. In-plane angle dependence of (a) R^{S}_{PHE} and (b) R^{AS}_{PHE} measured in a Hall bar in the presence of $H = 5$, 10, 20, 30, and 40 Oe. (c) In-plane field sweep of R^{S}_{PHE} and R^{AS}_{PHE} measured at $\phi_{current} = 135°$. (d) Out-of-plane field (H_z) dependence of antisymmetric Hall resistance (R^{AS}_{Hall}) measured with the in-plane magnetization held at selected angles by an in-plane bias field ($H_{xy} = 40$ Oe). Inset: Schematic of the out-of-plane field sweep configuration.

Figure S3(a) in the supplementary material shows that the APHE phase ϕ^{AS}_0 varies among nominally identical horizontal Hall bars patterned at relatively remote positions (more than 2 cm apart) across the same wafer. Because these Hall bars are identical in geometry and orientation, this observation suggests that local wafer-dependent structural variations, most likely strain, influence the APHE phase. To test this hypothesis, we tuned the interfacial strain by varying the seed layer beneath Ta/Py. Hall bars were fabricated from four wafers with the common stack Ta(5 nm)/Py(2 nm)/MgO(3 nm)/Ta(2 nm) grown on Si/SiO_2(100 nm) [SiO_2–100], Si/SiO_2(100 nm)/MgO(5 nm) [MgO–5], Si/SiO_2(100 nm)/Al_2O_3(20 nm) [Al_2O_3–20], and Si/SiO_2(100 nm)/Al_2O_3(40 nm) [Al_2O_3–40]. APHE is observed in all the wafers (Fig. S4 in the supplementary material); its amplitude R^{AS}_0 decreases for MgO–5, remains almost unchanged for Al_2O_3–20, and increases significantly when a thicker seed layer of alumina (Al_2O_3–40) is used (see Table I). All devices exhibit a small in-plane uniaxial anisotropy. Using the Stoner–Wohlfarth model, we extract the anisotropy field (H_k) and easy axis direction (ϕ_{easy}) as listed in Table I. Introducing MgO(5 nm) or Al_2O_3 (20 nm) slightly reduces H_k, whereas Al_2O_3 (40 nm) yields a pronounced reduction accompanied by a change in ϕ_{easy}.

A detailed analysis of the grazing-incidence x-ray diffraction (GI-XRD) confirms the seed layer-dependent out-of-plane contraction in the bottom Ta layer ($\epsilon_\perp < 0$, consistent with the in-plane tensile strain) with a clear trend: low $||\epsilon_\perp|| \Rightarrow$ lower H_k, and vice versa (see Table I and Subsec. S1.6, Figs. S6 and S7 in the supplementary material). Assuming that 10%–20% of the strain transfers into the 2 nm Py layer and contributes to a magnetoelastic anisotropy, the estimated change in H_k between the higher- and lower-strain seeds (SiO_2–100 vs Al_2O_3–40) could be in the order of 1.7–3.4 Oe, which is broadly compatible with the ~2.6 Oe reduction inferred from the PHE measurements. This suggests a seed-induced, magnetoelastic control of Py's in-plane anisotropy via strain. A thicker Al_2O_3 seed likely reduces lattice mismatch and stabilizes the Ta/Py stack, rotating ϕ_{easy} and further lowering H_k.

27 October 2026 10:58:36

© Author(s) 2026

TABLE I. Amplitude of the planar Hall resistance (R_0), easy axis direction (ϕ_{easy}), uniaxial anisotropy field (H_k), amplitude of APHE (R_0^{AS}), and the phase offset between the APHE peak and the easy axis ($||\phi_0^{AS} - \phi_{easy}||$) for Ta/Py layers grown on different seed layers. Lattice parameters (a and c) and out-of-plane and in-plane strain ($\epsilon_\perp, \epsilon_\parallel$) in bottom Ta layer.

	Transport and magnetic properties					Structural properties			
Wafer	R_0 (mΩ)	ϕ_{easy} (deg)	H_k (Oe)	R_0^{AS} (mΩ)	$\|\|\phi_0^{AS} - \phi_{easy}\|\|$ (deg)	a (Å)	c (Å)	$\epsilon_\perp$ (%)	$\epsilon_\parallel$ (%)
SiO_2–100	66.22	141.9	4.78	0.78	70.1	10.366	5.220	−1.78	−1.49
MgO–5	54.62	147.9	4.52	0.56	61.8	10.480	5.223	−1.73	−0.41
Al_2O_3–20	65.13	152.8	4.55	0.76	58.3	10.759	5.211	−1.97	2.25
Al_2O_3–40	53.41	162.5	2.21	1.36	6.5	10.439	5.244	−1.33	−0.79

A detailed analysis of the annealing effect is given in the supplementary material (Subsec. S1.7). Annealing causes a reduction in H_k in general and reduces $||\phi_0^{AS} - \phi_{easy}||$ except for Al_2O_3–40, which is already low in the as-grown state (Table S2 and Fig. S9 in the supplementary material). Its effect on R_{PHE}^{AS} is non-monotonic: it suppresses R_0^{AS} in the high-strain wafers (Al_2O_3–20, MgO–5, and SiO_2–100) but enhances it in the low-strain wafer (Al_2O_3–40). These results suggest that annealing, together with control of ϕ_{easy}, provides a route to tune R_0^{AS} and ϕ_0^{AS}.

Our measurements suggest that the most plausible origin of R_{PHE}^{AS} is an anomalous Hall contribution arising from a small perpendicular component of the magnetization. The fact that R_{PHE}^{AS} decreases as the Py layer is made thicker points to an interfacial source [Fig. S3(b) in the supplementary material]: as the film thickens, any interface-induced perpendicular magnetization is increasingly diluted by bulk Py, and its contribution correspondingly weakens.[49]

To account for the angular dependence of R_{PHE}^{AS}, we consider an interfacial DMI that couples the in-plane bulk spins to interfacial spins with a preferred chiral alignment. In a simple classical picture, the DMI energy is $H_{DM} = \vec{D} \cdot (\vec{S_1} \times \vec{S_2})$, where $\vec{D}$ is the DM vector, $\vec{S}_1$ represents a bulk (Py) spin, and $\vec{S}_2$ an interfacial spin (Fig. 4). For clarity, take $\vec{D} = D_x\hat{x}$ (in-plane) and constrain the bulk spin to the film plane, $\vec{S}_1 = S_{1x}\hat{x} + S_{1y}\hat{y}$. That makes $H_{DM} = D_x S_{1y} S_{2z}$, so the DMI selectively couples the in-plane y-component of the bulk spin to the out-of-plane z-component of the interfacial spin. Equivalently, the effective DM field (B_{DM}) acting on $\vec{S}_2$ along $\hat{z}$ scales as $S_{1y} \propto \sin\theta$, where θ is the angle between $\vec{D}$ (the x axis in this toy model) and the in-plane magnetization direction. This immediately yields the observed angular behavior: R_{PHE}^{AS} is maximized when the in-plane magnetization is perpendicular to $\vec{D}$ (i.e., when $\sin\theta$ is largest), because that is when the DMI most strongly induces an interfacial S_{2z} and thus the largest anomalous Hall-like contribution. Correlating this model with our results, we infer that the effective in-plane DM vector $\vec{D}$ is locally set by the interfacial strain and morphology and lies perpendicular to the direction of maximum APHE (ϕ_0^{AS}). While this model is simplified, its predictions for the phase and amplitude variations of R_{PHE}^{AS} are consistent with the data, lending support to an interfacial DMI origin.

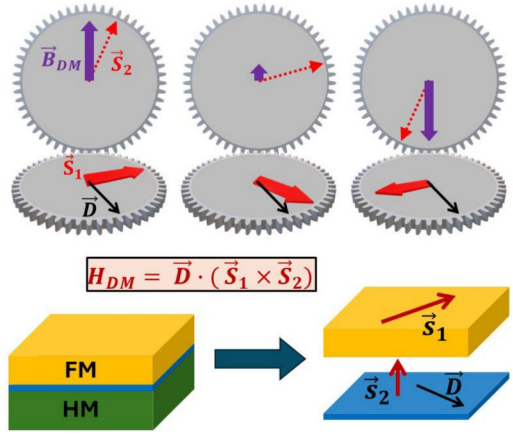


FIG. 4. A schematic representation of the in-plane control of interfacial perpendicular magnetization through DMI and an analogy with miter-gear rotation.

The observed phenomenon can be visualized analogously in Fig. 4 as a DMI miter gear where rotation of the in-plane magnetization drives an orthogonal interfacial response with a 1:1 gear ratio. Here, the radius vector of the horizontal wheel describes the direction of the in-plane magnetization, and the perpendicular projection of the radius vector of the standing wheel is proportional to the perpendicular magnetization. Since the remnant perpendicular magnetization can be tuned continuously by rotating the in-plane magnetization, this may open a new route to out-of-plane memory readout, which could increase the storage density of multilevel in-plane magnetic memory elements.

In summary, we have observed and systematically analyzed an APHE effect in Ta/Py bilayers. The data support the emergence of interfacial perpendicular magnetization driven by DMI. The magnitude and phase of the APHE are governed by the orientation of the in-plane bulk magnetization of Py. The APHE attains its maximum when the inferred DM vector is perpendicular to the in-plane magnetization. Our detailed analysis of seed layer, strain, and annealing effects suggests that the direction and strength of the interfacial DMI—and hence the perpendicular magnetization—can be controlled through strain engineering. This may offer a pathway to novel spintronic devices that exploit chirality-controlled, multistate memory functionality. Extending this study to other HM/FM bilayers will be important for establishing the generality of the phenomenon.

27 October 2026 10:58:36

© Author(s) 2026

See the supplementary material, available from the journal's online library or from the authors. It includes PHE data measured in two different configurations and their decomposition into SPHE and APHE (Fig. S1); additional understanding of the exclusion of spin–orbit torque (SOT) contributions (Fig. S2); the role of the substrate and a thicker Py layer (Fig. S3); APHE across wafers with different seed layers (Fig. S4); fits to the PHE on-off data (Fig. S5); detailed analysis on GI-XRD data to extract strain and its relation with magnetic anisotropy (Figs. S6 and S7); and the effect of annealing on magnetic anisotropy and APHE (Figs. S8 and S9).

L.K. and S.C. acknowledge support from the Multispin.AI project, which has received funding from EU under Grant Agreement No. 101130046. "Funded by the European Union. Views and opinions expressed are however those of the author(s) only and do not necessarily reflect those of the European Union or the European Innovation Council and SMEs Executive Agency (EISMEA). Neither the European Union nor the granting authority can be held responsible for them." S.C. acknowledges funding through FCT with Reference No. UID/PRR/05367/2025, DOI: https://doi.org/10.54499/UID/PRR/05367/2025.

AUTHOR DECLARATIONS

Conflict of Interest

The authors have no conflicts to disclose.

Author Contributions

A. Ghosh: Conceptualization (equal); Data curation (lead); Formal analysis (lead); Investigation (lead); Methodology (equal); Software (lead); Supervision (supporting); Validation (equal); Visualization (equal); Writing – original draft (lead); Writing – review & editing (lead). **A. Zaig:** Conceptualization (equal); Data curation (supporting); Formal analysis (supporting); Investigation (equal); Methodology (equal); Software (supporting); Validation (supporting); Visualization (equal); Writing – original draft (supporting); Writing – review & editing (supporting). **D. B. C. Gonçalves:** Conceptualization (supporting); Formal analysis (supporting); Methodology (equal); Visualization (supporting); Writing – original draft (supporting); Writing – review & editing (supporting). **S. Cardoso:** Conceptualization (supporting); Funding acquisition (equal); Investigation (supporting); Methodology (supporting); Project administration (equal); Resources (equal); Supervision (equal); Validation (equal); Visualization (supporting); Writing – review & editing (supporting). **L. Klein:** Conceptualization (equal); Formal analysis (equal); Funding acquisition (lead); Investigation (equal); Methodology (supporting); Project administration (lead); Resources (lead); Supervision (lead); Validation (lead); Visualization (equal); Writing – original draft (supporting); Writing – review & editing (equal).

DATA AVAILABILITY

The data that support the findings of this study are available from the corresponding author upon reasonable request.

REFERENCES

[1]W. Skowroński, T. Nozaki, D. D. Lam, Y. Shiota, K. Yakushiji, H. Kubota, A. Fukushima, S. Yuasa, and Y. Suzuki, "Underlayer material influence on electric-field controlled perpendicular magnetic anisotropy in CoFeB/MgO magnetic tunnel junctions," Phys. Rev. B **91**, 184410 (2015).
[2]J. Sinha, M. Hayashi, A. J. Kellock, S. Fukami, M. Yamanouchi, H. Sato, S. Ikeda, S. Mitani, S. Yang, S. S. P. Parkin, and H. Ohno, "Enhanced interface perpendicular magnetic anisotropy in Ta|CoFeB|MgO using nitrogen doped Ta underlayers," Appl. Phys. Lett. **102**, 242405 (2013).
[3]Y. Shiota, T. Nozaki, F. Bonell, S. Murakami, T. Shinjo, and Y. Suzuki, "Induction of coherent magnetization switching in a few atomic layers of FeCo using voltage pulses," Nat. Mater. **11**, 39 (2012).
[4]V. Sokalski, M. T. Moneck, E. Yang, and J.-G. Zhu, "Optimization of Ta thickness for perpendicular magnetic tunnel junction applications in the MgO–FeCoB–Ta system," Appl. Phys. Lett. **101**, 072411 (2012).
[5]W. Zhang, W. Han, X. Jiang, S.-H. Yang, and S. S. P. Parkin, "Role of transparency of platinum–ferromagnet interfaces in determining the intrinsic magnitude of the spin Hall effect," Nat. Phys. **11**, 496 (2015).
[6]C. Swindells, H. Głowiński, Y. Choi, D. Haskel, P. P. Michałowski, T. Hase, F. Stobiecki, P. Kuświk, and D. Atkinson, "Magnetic damping in ferromagnetic/heavy-metal systems: The role of interfaces and the relation to proximity-induced magnetism," Phys. Rev. B **105**, 094433 (2022).
[7]C.-F. Pai, M. Maxwell, A. J. Tan, and G. S. D. Beach, "Determination of spin torque efficiencies in heterostructures with perpendicular magnetic anisotropy," Phys. Rev. B **93**, 144409 (2016).
[8]C. Y. Hu, W. D. Chen, Y. T. Liu, C.-C. Huang, and C.-F. Pai, "The central role of tilted anisotropy for field-free spin–orbit torque switching of perpendicular magnetization," NPG Asia Mater. **16**(1), 1 (2024).
[9]T. Jungwirth, J. Wunderlich, and K. Olejník, "Spin Hall effect devices," Nat. Mater. **11**, 382–390 (2012).
[10]W. Zhang, M. B. Jungfleisch, W. Jiang, Y. Liu, J. E. Pearson, S. G. E. te Velthuis, A. Hoffmann, F. Freimuth, and Y. Mokrousov, "Reduced spin-Hall effects from magnetic proximity," Phys. Rev. B **91**, 115316 (2015).
[11]O. Inyang, L. Bouchenoire, B. Nicholson, M. Tokaç, R. M. Rowan-Robinson, C. J. Kinane, and A. T. Hindmarch, "Threshold interface magnetization required to induce magnetic proximity effect," Phys. Rev. B **100**, 174418 (2019).
[12]M. Kuepferling, A. Casiraghi, G. Soares, G. Durin, F. Garcia-Sanchez, L. Chen, C. H. Back, C. H. Marrows, S. Tacchi, and G. Carlotti, "Measuring interfacial Dzyaloshinskii–Moriya interaction in ultrathin magnetic films," Rev. Mod. Phys. **95**, 015003 (2023).
[13]K. Zakeri, Y. Zhang, J. Prokop, T.-H. Chuang, N. Sakr, W. X. Tang, and J. Kirschner, "Asymmetric spin-wave dispersion on Fe(110): Direct evidence of the Dzyaloshinskii–Moriya interaction," Phys. Rev. Lett. **104**, 137203 (2010).
[14]F. Hellman, A. Hoffmann, Y. Tserkovnyak, G. S. D. Beach, E. E. Fullerton, C. Leighton, A. H. MacDonald, D. C. Ralph, D. A. Arena *et al.*, "Interface-induced phenomena in magnetism," Rev. Mod. Phys. **89**, 025006 (2017).
[15]J. H. Moon, S.-M. Seo, K.-J. Lee, K.-W. Kim, J. Ryu, H.-W. Lee, R. D. McMichael, and M. D. Stiles, "Spin-wave propagation in the presence of interfacial Dzyaloshinskii–Moriya interaction," Phys. Rev. B **88**, 184404 (2013).
[16]Y. Tokura and N. Kanazawa, "Magnetic skyrmion materials," Chem. Rev. **121**, 2857–2897 (2021).
[17]B. Göbel, I. Mertig, and O. A. Tretiakov, "Beyond skyrmions: Review and perspectives of alternative magnetic quasiparticles," Phys. Rep. **895**, 1–28 (2021).
[18]T. Zhou, S. Zhou, X. Xie, X. Zhao, Y. Dong, J. Wang, W. Chen, Q. Leng, L. Bai, Y. Chen, S. Kang, Y. Liu, S. Yan, and Y. Tian, "Perpendicular effective field induced by spin–orbit torque and magnetization damping in chiral domain walls," Phys. Rev. B **107**, 104411 (2023).
[19]J. Yu, X. Qiu, Y. Wu, J. Yoon, P. Deorani, J. M. Besbas, A. Manchon, and H. Yang, "Spin orbit torques and Dzyaloshinskii–Moriya interaction in dual-interfaced Co–Ni multilayers," Sci. Rep. **6**, 32629 (2016).
[20]M. Belmeguenai, M. S. Gabor, Y. Roussigné, A. Stashkevich, S. M. Chérif, F. Zighem, and C. Tiusan, "Brillouin light scattering investigation of the thickness dependence of Dzyaloshinskii–Moriya interaction in $Co_{0.5}Fe_{0.5}$ ultrathin films," Phys. Rev. B **93**, 174407 (2016).
[21]J. A. Arregi, P. Riego, A. Berger, and E. Y. Vedmedenko, "Large interlayer Dzyaloshinskii–Moriya interactions across Ag-layers," Nat. Commun. **14**, 6927 (2023).
[22]J. Liang, M. Chshiev, A. Fert, and H. Yang, "Gradient-induced Dzyaloshinskii–Moriya interaction," Nano Lett. **22**, 10128–10133 (2022).

27 October 2026 10:58:36

© Author(s) 2026

[23]C. Deger, "Strain-enhanced Dzyaloshinskii–Moriya interaction at Co/Pt interfaces," Sci. Rep. **10**, 12314 (2020).
[24]X. Ma, G. Yu, X. Li, T. Wang, D. Wu, K. S. Olsson, Z. Chu, K. An, J. Q. Xiao, K. L. Wang, and X. Li, "Interfacial control of Dzyaloshinskii–Moriya interaction in heavy metal/ferromagnetic metal thin film heterostructures," Phys. Rev. B **94**, 180408 (2016).
[25]D. de Souza Chaves, F. Ajejas, V. Křižáková, J. Voges, and S. Pizzini, "Oxidation dependence of the Dzyaloshinskii–Moriya interaction in Pt/Co/MO_x trilayers (M=Al or Gd)," Phys. Rev. B **99**, 144404 (2019).
[26]V. L. Zhang, K. Di, H. S. Lim, S. C. Ng, M. H. Kuok, J. Yu, J. Yoon, X. Qiu, and H. Yang, "In-plane angular dependence of the spin-wave nonreciprocity of an ultrathin film with Dzyaloshinskii–Moriya interaction," Appl. Phys. Lett. **107**, 022402 (2015).
[27]K. Ahmadi, F. Mahfouzi, L. Jamilpanah, M. Mohseni, T. Böttcher, P. Pirro, N. Kioussis, J. Åkerman, S. A. S. Ebrahimi, and S. M. Mohseni, "Inducing Dzyaloshinskii–Moriya interaction in symmetrical multilayers using post annealing," Sci. Rep. **12**, 11877 (2022).
[28]G. Chen, M. Robertson, H. Kwon, C. Won, A. K. Schmid, and K. Liu, "Chirality-induced zigzag domain wall in in-plane magnetized ultrathin films," J. Vac. Sci. Technol., A **39**, 053410 (2021).
[29]K. Karube, L. Peng, J. Masell, X. Yu, F. Kagawa, Y. Tokura, and Y. Taguchi, "Room-temperature antiskyrmions and sawtooth surface textures in a noncentrosymmetric magnet with S_4 symmetry," Nat. Mater. **20**, 335–340 (2021).
[30]M. Robertson, C. J. Agostino, G. Chen, S. P. Kang, A. Mascaraque, E. G. Michel, C. Won, Y. Wu, and A. K. Schmid, "In-plane Néel wall chirality and orientation of interfacial Dzyaloshinskii–Moriya vector in magnetic films," Phys. Rev. B **102**, 024417 (2020).
[31]R. Battilomo, N. Scopigno, and C. Ortix, "Anomalous planar Hall effect in two-dimensional trigonal crystals," Phys. Rev. Res. **3**, L012006 (2021).
[32]H. Tan, Y. Liu, and B. Yan, "Unconventional anomalous Hall effect from magnetization parallel to the electric field," Phys. Rev. B **103**, 214438 (2021).
[33]J. Cao, W. Jiang, X.-P. Li, D. Tu, J. Zhou, J. Zhou, and Y. Yao, "In-plane anomalous Hall effect in $\mathcal{PT}$-symmetric antiferromagnetic materials," Phys. Rev. Lett. **130**, 166702 (2023).
[34]J. Zhou, W. Zhang, Y.-C. Lin *et al.*, "Heterodimensional superlattice with in-plane anomalous Hall effect," Nature **609**, 46–51 (2022).
[35]P. Li, C. Zhang, Y. Wen, L. Cheng, G. Nichols, D. G. Cory, G.-X. Miao, and X.-X. Zhang, "Anomalous planar Hall effect in the type-II topological Weyl semimetal WTe_2," Phys. Rev. B **100**, 205128 (2019).
[36]T. Liang, J. Lin, Q. Gibson *et al.*, "Anomalous Hall effect in $ZrTe_5$," Nat. Phys. **14**, 451–455 (2018).
[37]J. Ge, D. Ma, and Y. Liu, "Unconventional Hall effect induced by Berry curvature," Natl. Sci. Rev. **7**, 1879–1885 (2020).
[38]Y. Wang, P. A. Lee, D. M. Silevitch, F. Gomez, S. E. Cooper, Y. Ren, J.-Q. Yan, D. Mandrus, T. F. Rosenbaum, and Y. Feng, "Antisymmetric linear magnetoresistance and the planar Hall effect," Nat. Commun. **11**, 216 (2020).
[39]Y. Cui, Z. Li, H. Chena, Y. Wu, Y. Chen, K. Peie, T. Wu, N. Xie, R. Chee, X. Qiu, Y. Liu, Z. Yuan, and Y. Wu, "Antisymmetric planar Hall effect in rutile oxide films induced by the Lorentz force," Sci. Bull. **69**, 2362–2369 (2024).
[40]J. Singh, K. V. Raman, and N. Mohanta, "Anisotropic planar Hall effects in Bi_2Se_3/EuS interfaces: Deciphering the role of proximity-induced spin canting and topological spin texture," Phys. Rev. B **110**, 125133 (2024).
[41]S. Das, A. Zaig, M. Schultz, and L. Klein, "Stabilization of exponential number of discrete remanent states with localized spin–orbit torques," Appl. Phys. Lett. **116**, 262405 (2020).
[42]H. Yan, G. J. Omar, Z. Zhang, Z. S. Lim, and A. Ariando, "High-quality NiFe thin films on oxide/non-oxide platforms via pulsed laser deposition at room temperature," Adv. Mater. Inter. **11**, 2300265 (2024).
[43]Y.-T. Chen, S. Takahashi, H. Nakayama, M. Althammer, S. T. B. Goennenwein, E. Saitoh, and G. E. W. Bauer, "Theory of spin Hall magnetoresistance (SMR) and related phenomena," J. Phys.: Condens. Matter **28**, 103004 (2016).
[44]S. Seri and L. Klein, "Antisymmetric magnetoresistance of the $SrTiO_3$/$LaAlO_3$ interface," Phys. Rev. B **80**, 180410 (2009).
[45]M. Büttiker, "Symmetry of electrical conduction," IBM J. Res. Dev. **32**, 317 (1988).
[46]C. Safranski, E. A. Montoya, and I. N. Krivorotov, "Spin–orbit torque driven by a planar Hall current," Nat. Nanotechnol. **14**, 27–30 (2019).
[47]S. A. Razavi, D. Wu, G. Yu, Y.-C. Lau, K. L. Wong, W. Zhu, C. He, Z. Zhang, J. M. D. Coey, P. Stamenov, P. K. Amiri, and K. L. Wang, "Joule heating effect on field-free magnetization switching by spin-orbit torque in exchange-biased systems," Phys. Rev. Appl. **7**, 024023 (2017).
[48]D. Li, S. Chen, Y. Zuo, J. Yun, B. Cui, K. Wu, X. Guo, D. Yang, J. Wang, and L. Xi, "Roles of joule heating and spin–orbit torques in the direct current induced magnetization reversal," Sci. Rep. **8**, 12959 (2018).
[49]S. Husain, S. Pal, X. Chen *et al.*, "Large Dzyaloshinskii–Moriya interaction and atomic layer thickness dependence in a ferromagnet–WS_2 heterostructure," Phys. Rev. B **105**, 064422 (2022).

27 October 2026 10:58:36

© Author(s) 2026